Photoacoustic investigation of transport in semiconductors: Theoretical and experimental study of a Ge single crystal

M. D. Dramićanin
Institute of Nuclear Sciences "VINČA", Laboratory for Radiation Chemistry and Physics "GAMMA", P.O. Box 522, 11001 Belgrade, Yugoslavia

Z. D. Ristovski
Faculty of Electrical Engineering, University of Belgrade, 11000 Belgrade, P.O. Box 816, Yugoslavia

P. M. Nikolić
Institute of Technical Sciences of SASA, Knez Mihajlova 35, Belgrade, Yugoslavia

D. G. Vasiljević and D. M. Todorović
Joint Laboratory for Advanced Materials of SASA and CMS, 11000 Belgrade, P.O. Box 373, Yugoslavia

(Received 16 September 1994)

Photoacoustic (PA) heat-transmission measurements were used to study transport in a nearly intrinsic Ge single crystal. A theoretical model was developed which quantitatively describes excess carrier and thermal-wave space distributions, within the semiconductor under monochromatic cw modulated excitation. The PA heat-transmission, reflection, and photothermal-beam-deflection signals can be calculated using this model. It is shown that the frequency characteristic of the measurement system can be eliminated using measurements on different thicknesses of the same sample. It is also shown that both the normalized phase and amplitude spectra, as a function of the modulation frequency, can be used to determine the values of the thermal diffusivity, the excess-carrier lifetime, and the surface recombination velocity.

I. INTRODUCTION

Photoacoustic (PA) and photothermal effects have become terms used to describe the generation of acoustic waves and other thermoelastic effects in material under light excitation. The material is usually irradiated by a modulated light beam, which is then absorbed by the sample and converted into heat. The heat diffuses to the sample surface and then into the surrounding gas atmosphere of the photoacoustic cell. Finally, the thermal expansion of the gas generates the photoacoustic signal. Thus, the absorption of a modulated light beam at any point in the sample results in a periodic localized heating of the medium. The heat energy is transmitted to the surrounding matter by conduction and diffusion.

During the past few years various properties of semiconductors were intensively investigated, using PA signal measurements.[1-3] At the beginning only thermal diffusivity of semiconductors was measured,[4] using PA signal amplitude measurements as a function of the modulation frequency. Fournier *et al.*[5] extended the approach of photothermal deflection to investigate transport properties of semiconductors which yielded the thermal diffusivity, the electronic diffusivity, the excess-carrier lifetime, and the surface recombination velocity and Pelzl *et al.*[6] report time and spatially resolved investigation of transport in semiconductors by the mirage effect. Then, more recently, using photoacoustic phase measurements in heat-transmission configuration, carrier transport properties (carrier-diffusion coefficient, surface recombination velocity and mean recombination time) together with the thermal diffusivity of PbTe,[7] GaAs, and Si solar cells[8] were investigated. In these papers the authors used the thermal piston model of Rosencwaig and Gersho (RG model[9]). They calculated the PA signal at the rear surface of the sample including the absorption process on the front side and the mechanism of both surface and bulk recombination and thermal diffusion.

In this paper an improved model of PA signal generation in semiconductors is developed. Expressions for the distributions of the periodic parts of the thermal flux due to three principal thermal sources (thermalization, nonradiative surface, and bulk recombination) are analytically evaluated enabling calculation of the PA signal amplitude and phase at the front and rear surfaces of the sample. Theoretical results are compared with experimental data, obtained with Ge single crystal samples, and they are in good agreement.

II. THEORETICAL MODEL

A one-dimensional model (Fig. 1) which predicts the PA amplitude and phase was developed allowing the determination of both thermal and electronic transport properties of intrinsic or near intrinsic semiconductors. In this model the optical absorption coefficient is treated as finite. In that case the absorption occurs throughout the sample volume rather than just being a surface absorption process. A one-dimensional treatment is sufficient if one considers the case where the front face is uniformly illuminated by a laser beam whose dimensions are much larger than both the thermal diffusion and the carrier-diffusion lengths. Under monochromatic light excitation of the semiconductor, modulated at an angular frequency ω, the flux of photons penetrating to depth x

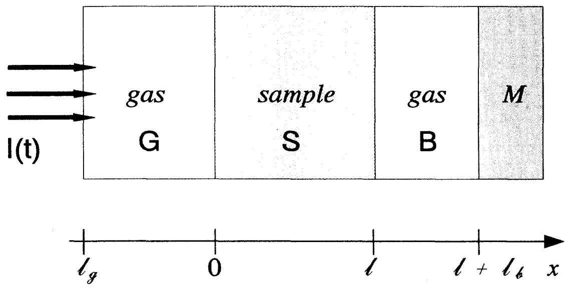

FIG. 1. PA cell geometry for the heat-transmission configuration.

in the sample is given by

$$I(x,\omega,t) = \frac{I_0}{2} e^{-\alpha x} \mathrm{Re}\left[1 + e^{j\omega t}\right], \tag{1}$$

where I_0 is the intensity of the incident light and α is the optical absorption coefficient of the photoexcited semiconductor at the excitation wavelength.

It is assumed that the energy of the excitation beam E is greater than the band gap energy of the semiconductor E_g. To evaluate the excess carrier distribution we made the following assumptions: charge balance (i.e., the excess free electron density is equal to the excess free hole density), the sample is uniformly doped so the gradients and time derivates of n and p are simply equal to the gradients and time derivates of δn and δp, and the carrier lifetime is independent of the free carrier concentration (Auger recombination will be neglected).

Under these assumptions, the carrier-diffusion equations are linear in both δn and δp, and therefore the components of δn and δp at a given temporal modulation frequency ω may be solved independently, using the component of the incident radiation at the modulation frequency ω as the driving source of the photocarrier generation. Here, the equation governing the photocarrier generation and diffusion at the modulation frequency ω in the semiconductor may be written in the form

$$\frac{d^2\delta n(x)}{dx^2} - \frac{1}{L_D^2}\delta n(x) = -\frac{\alpha I_0}{2ED} e^{-\alpha x} \tag{2}$$

with the boundary conditions

$$\begin{aligned} D\frac{d(\delta n(x))}{dx}|_{x=0} &= s_g \delta n(0), \\ D\frac{d(\delta n(x))}{dx}|_{x=l} &= -s_b \delta n(l), \end{aligned} \tag{3}$$

where $L_D = \sqrt{D\tau/(1+j\omega\tau)}$ is the complex mean diffusion length of excess carriers, s_g, s_b are front and rear surface recombination velocities, and τ is the excess-carrier lifetime within the bulk. In our experiments we have used a lightly doped germanium sample ($N_d \sim 10^{14}$ cm^{-3}, $\rho = 20\ \Omega$ cm), so we can assume that the ambipolar diffusion coefficient of excess carriers is $D = 2D_nD_p/(D_n + D_p)$.[10]

The general solution of Eq. (2) with boundary conditions Eq. (3) is

$$\delta n(x) = K\left(B_1 e^{x/L_D} + B_2 e^{-x/L_D} - e^{-\alpha x}\right), \tag{4}$$

where

$$\begin{aligned} K &= \frac{I_0}{2ED}\frac{\alpha}{\alpha^2 - 1/L_D^2}, \\ B_1 &= \frac{(\eta_g+1)(\epsilon_b-1)e^{-l/L_D} - (\eta_b-1)(\epsilon_g+1)e^{-\alpha l}}{(\epsilon_g+1)(\epsilon_b+1)e^{l/L_D} - (\epsilon_g-1)(\epsilon_b-1)e^{-l/L_D}}, \\ B_2 &= \frac{(\eta_g+1)(\epsilon_b+1)e^{l/L_D} - (\eta_b-1)(\epsilon_g-1)e^{-\alpha l}}{(\epsilon_g+1)(\epsilon_b+1)e^{l/L_D} - (\epsilon_g-1)(\epsilon_b-1)e^{-l/L_D}}, \end{aligned} \tag{5}$$

and $\eta_{g(b)} = \epsilon_{g(b)}\alpha L_D$, $\epsilon_{g(b)} = D/L_D s_{g(b)}$.

The quantity $\epsilon_{g(b)}$ represents the ratio of the bulk diffusion velocity (D/L_D) and the interfacial recombination velocity ($s_{g(b)}$). For a completely reflecting boundary $\epsilon_{g(b)} = \infty$, an Ohmic contact is characterized by $\epsilon_{g(b)} = 0$ and $\epsilon \sim 1$ describes an interface which cannot be distinguished from a continuation of the bulk material.

The distribution of the periodic part of the thermal flux Θ can be obtained by solving the following system of differential equations:

$$\left[\frac{d^2}{dx^2} - \sigma_i^2\right]\Theta_i = \begin{cases} 0, & i = g, b \\ -Q(x), & i = s \end{cases} \tag{6}$$

where $\sigma_i^2 = j\omega/D_{Ti}$, D_{Ti} is the thermal diffusivity of the layer i, and s, g, and b denote "sample," "gas," and "backing," respectively.

The thermal sources in the sample, $Q(x)$, may be regarded as due to three different processes, the first due to the immediate thermalization (T) of carriers to the band gap, the second due to nonradiative recombination (band to band) of the photoexcited carriers that have diffused into the semiconductor (NRR), and the third due to nonradiative surface recombination (SR). The first two are incorporated in the unhomogeneous part of the thermal diffusion equation (6), and can be described as follows:

$$\begin{aligned} Q(x) &= Q_T(x) + Q_{\mathrm{NRR}}(x) \\ &= \frac{\alpha I_0}{2k_s}\frac{E-E_g}{E}e^{-\alpha x} + \frac{E_g}{k_s\tau}\delta n(x), \end{aligned} \tag{7}$$

where k_s is thermal conductivity. The third part Q_{SR} is incorporated in the boundary conditions:

$$\begin{aligned} \Theta_g(0) &= \Theta_s(0), \\ \Theta_s(l) &= \Theta_b(l), \\ -k_s\frac{d\Theta_g(x)}{dx}|_{x=0} &= -k_g\frac{d\Theta_s(x)}{dx}|_{x=0} + s_g\delta n(0)E_g, \\ -k_b\frac{d\Theta_s(x)}{dx}|_{x=l} &= -k_s\frac{d\Theta_b(x)}{dx}|_{x=l} + s_b\delta n(l)E_g. \end{aligned} \tag{8}$$

The solution of the thermal diffusion equation (6) with the boundary conditions (8) leads to the following expression for the distribution of the periodic part of the thermal flux in the sample:

$$\Theta_S(x) = \Theta_T(x) + \Theta_{\mathrm{NRR}}(x) + \Theta_{\mathrm{SR}}(x) \tag{9}$$

with

$$\Theta_T(x) = \frac{I_0}{2k_s}\frac{E-E_g}{E}\frac{\alpha}{\alpha^2-\sigma_s^2} \times \left[\frac{(g+r)(1-b)e^{\sigma_s(x-l)}+(g+r)(1+b)e^{-\sigma_s(x-l)}+(b-r)e^{-\alpha l}\left[(1+g)e^{\sigma_s x}+(1-g)e^{-\sigma_s x}\right]}{(1+g)(1+b)e^{\sigma_s l}-(1-g)(1-b)e^{-\sigma_s l}} - e^{-\alpha x}\right], \tag{10a}$$

$$\Theta_{\rm SR}(x) = \frac{2E_g}{k_s\sigma_s}\frac{s_g\delta n(0)\left\{\cosh[\sigma_s(x-l)]-b\sinh[\sigma_s(x-l)]\right\}+s_b\delta n(l)\left[\cosh(\sigma_s x)+g\sinh(\sigma_s x)\right]}{(1+g)(1+b)e^{\sigma_s l}-(1-g)(1-b)e^{-\sigma_s l}}, \tag{10b}$$

$$\Theta_{\rm NRR}(x) = \frac{KE_g}{k_s\tau\sigma_s^2}\left\{\frac{C_1e^{\sigma_s x}+C_2e^{-\sigma_s x}}{(1+g)(1+b)e^{\sigma_s l}-(1-g)(1-b)e^{-\sigma_s l}} - \frac{1}{m^2-1}\left[\frac{\delta n(x)}{K}+\frac{r^2-m^2}{r^2-1}e^{-\alpha x}\right]\right\}, \tag{10c}$$

with

$$C_1 = (V_3+gV_1)(1-b)e^{-\sigma_s l}+(V_4+bV_2)(1+g),$$
$$C_2 = (V_3-gV_1)(1+b)e^{\sigma_s l}+(V_4+bV_2)(1-g),$$

and

$$V_1 = -\frac{\delta n(0)/K+1}{m^2-1}+\frac{1}{r^2-1},$$
$$V_2 = \frac{\delta n(l)/K+e^{-\alpha l}}{m^2-1}-\frac{e^{-\alpha l}}{r^2-1},$$
$$V_3 = -m\frac{\frac{1}{K}\left[\delta n(l)-\delta n(0)\cosh(l/L_D)\right]-\cosh(l/L_D)+e^{-\alpha l}}{\sinh(l/L_D)(m^2-1)}-\frac{r}{r^2-1},$$
$$V_4 = m\frac{\frac{1}{K}\left[\delta n(l)\cosh(l/L_D)-\delta n(0)\right]-1+e^{-\alpha l}\cosh(l/L_D)}{\sinh(l/L_D)(m^2-1)}+\frac{re^{-\alpha l}}{r^2-1},$$

where $g(b) = k_{g(b)}\sigma_{g(b)}/k_s\sigma_s$, $r = \alpha/\sigma_s$, and $m = 1/L_D\sigma_s$; T, NRR, and SR represent components of the sample temperature fluctuations at any point in the sample, respectively.

Depending on the position of the microphone there exists two possible detection configurations: the microphone is at the front illuminated surface and at the rear, opposite surface.

The well-known RG expression for the periodic part of the thermal flux can be easily obtained from our theoretical outcome if one substitutes $x = 0$ into Eq. (10a).

When the microphone is at the rear surface, as in our experimental setup, and according to the thermal-piston model of RG, the pressure fluctuation δP in the gas region, due to the periodic heating of the sample, is given by

$$\delta P = \frac{\kappa P_0\Theta_s(l)}{T_0 l_b\sigma_b}e^{j\omega t}, \tag{11}$$

where P_0 (T_0) is the ambient pressure (temperature), l_b the length of the gas chamber, σ_b is the thermal diffusion coefficient in the backing, in our case air, and $\Theta_s(l)$ is the sample temperature fluctuation at the $x = l$ sample-backing (gas) interface.

For the case of short-wavelength incident radiation, as is the case in our experiment, we may assume that $\exp(-\alpha l) \simeq 0$. If we also neglect the heat flow into the surrounding gas, $g = b \simeq 0$, Eq. (10a) can be written in the following form:

$$\Theta_T(l) = \frac{E-E_g}{E}\frac{I_0}{2k_s\sigma_s}\frac{1}{\sinh(\sigma_s l)}, \tag{12a}$$

$$\Theta_{\rm NRR}(l) = \frac{E_g}{E}\frac{I_0F}{k_s\tau\sigma_s^2}\frac{1}{m^2-1}\left\{\frac{m\frac{D}{L_D}\sinh(l/L_D)-ms_b\cosh(l/L_D)}{\sinh(\sigma_s l)}+ms_b\coth(\sigma_s l)-\frac{D}{L_D}\right\}, \tag{12b}$$

$$\Theta_{\rm SR}(l) = \frac{E_g}{E}\frac{I_0F}{k_s\sigma_s}\left\{\frac{s_g}{\sinh(\sigma_s l)}\left(\frac{D}{L_D}\cosh(l/L_D)-s_b\sinh(l/L_D)\right)+\frac{D}{L_D}\frac{s_b}{\tanh(\sigma_s l)}\right\}, \tag{12c}$$

where

$$F = \frac{1}{(D/L_D+s_g)(D/L_D+s_b)e^{l/L_D}-(D/L_D-s_g)(D/L_D-s_b)e^{-l/L_D}}. \tag{13}$$

Equations written in this form are much easier to discuss than in the full form Eq. (10a). The first terms in both Eqs. (12b) and (12c) present the thermal contribution to the recombination components, while the second terms present the carrier transport contribution to the recombination components.

At lower frequencies, the material is thermally thin and the thermalization component is dominant, and consequently the signal exhibits "pure" thermal wave behavior in both the amplitude and phase, the frequency dependence of the signal is governed by $1/\sigma_b\sigma_s \sinh(\sigma_s l)$. In this frequency region, as a consequence of $1/\sigma_s > L_D$, the thermal contribution to the recombination components, first terms in Eq. (12b) and Eq. (12c), is dominant. This is the case up to those frequencies where the thermal diffusion length is roughly five times the sample thickness. For higher frequencies the sample becomes thermally thick $e^{-\sigma_s l} \approx 0$ and the first terms in these equations vanish. For these frequencies the carrier transport contribution to the recombination components Θ_{SR} and Θ_{NRR} becomes dominant, as the condition $1/\sigma_s < L_D$ is fulfilled. These contributions were previously considered in photothermal deflection technique by Fournier *et al.*[5]

III. EXPERIMENTAL RESULTS

The experiments were performed using a similar configuration to the so-called open-photoacoustic cell (OPC). The main difference between the OPC configuration and the one we used was that our sample was firmly pressed to the sound inlet, which was a hole of $d = 2$ mm. In the OPC configuration the sample was also mounted directly onto a circular electret microphone but it was fixed only with vacuum grease. The construction of the cell was very similar to that presented by Pinto Neto *et al.*[7] The inner diameter of the cell was 10 mm and the distance between the back sample surface and the metalized membrane was ~1.5 mm. The light source was a 15 mW HeNe laser and a mechanical chopper was used for beam modulation.

Measurements were made using n-type single crystals with a specific resistivity of $\rho \sim 20\ \Omega$ cm, at room temperature. As one can see from the value of the specific resistivity the sample was nearly intrinsic. To investigate the influence of the surface recombination the sample surfaces were specially prepared. The sample surface in contact with air in the PA chamber, opposite to the illuminated surface, was highly polished. This mirror-like polished surface finish was obtained by a sequence of mechanical polishing procedures. Ge samples of different thicknesses were obtained by thinning the roughened side of the starting sample. The thickness of the starting sample was $d_1 = 1000\ \mu$m and it was thinned down to $d_2 = 910\ \mu$m and $d_3 = 770\ \mu$m. In all three measurements the polished side was in contact with the air of the PA chamber.

The PA amplitude and phase as a function of the modulation frequency, for all three thicknesses, are shown in Figs. 2 and 3, respectively. As we decrease the sample thickness the minimum in the PA phase moved to higher frequencies, from 250 Hz for the 1000 μm to 370 Hz for the 770 μm thickness. Similarly for the breaking frequency (f_c), the frequency at which the amplitude changed its slope from $\exp(-a\sqrt{f})/f$ to f^{-v}, where $a = d\sqrt{\pi/D_T}$ and v =1–2, altered from 250 Hz for the 1000 μm to 370 Hz for the 770 μm thick sample. As the sample was made thinner it became thermally thick at higher frequencies and the recombination component, either bulk or surface, became dominant. The place of the minimum in the phase was roughly at those frequencies where the sample thermal diffusion length $(D_T/\pi f)^{1/2}$ became five times smaller than the sample thickness. For frequencies smaller than the breaking frequency f_c the thermal component was dominant — the slope of the amplitude was $\exp(-a\sqrt{f})/f$ and the phase slope was $-a\sqrt{f}$. For frequencies higher than f_c the recombination component became dominant and the slope of the amplitude changed to $f^{-1.05}$.

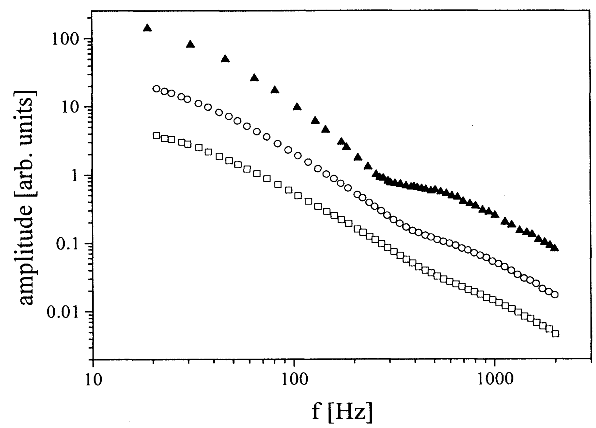

FIG. 2. Experimental PA signal amplitude vs modulation frequency for three sample thicknesses: 1000 (triangles), 910 (circles), and 710 μm (squares).

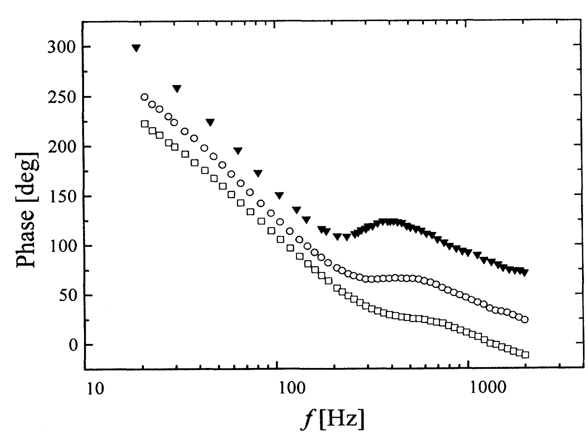

FIG. 3. Experimental PA signal phase angle vs modulation frequency for three Ge sample thicknesses: 1000 (triangles), 910 (circles), and 710 μm (squares).

IV. DISCUSSION

The PA signal, measured by a lock-in amplifier, can be presented as a vector rotating in a complex plain:

$$S(\omega) = F_T(\omega)\delta P(\omega), \tag{14}$$

where $F_T(\omega)$ represents the complex frequency characteristics of the whole measuring system (chopper, PA cell with the influence of the microphone, lock-in, etc.); $\delta P(\omega)$ is the complex preasure variation Eq. (11).

In most PA measurements with the conventional PA cell, where the microphone is at the front illuminated surface of the sample, one can use carbon black to normalize the measured signal, because carbon black is an excellent absorber and thermally thin, so the PA amplitude and phase are saturated and independent of the optical and thermal characteristics of the sample. In our detection configuration such normalization is not possible. To eliminate the influence of the measuring system we had to normalize our signal in a different way. We used PA measurements of the same sample at two different thicknesses. Using Eqs. (9), and (11) the signal ratio for two different thicknesses can be presented as

$$\begin{aligned} R_{12} &= \frac{S_1}{S_2} = \frac{\delta P_1}{\delta P_2} = \frac{\Theta_s(l_1)}{\Theta_s(l_2)} \\ &= \frac{|\Theta_s(l_1)|}{|\Theta_s(l_2)|} \exp\{j[\phi_s(l_1) - \phi_s(l_2)]\} = A_r e^{j\Delta\phi}, \end{aligned} \tag{15}$$

where $\phi_s(l_1)$ and $\phi_s(l_2)$ are the phase angles of the measured PA signal for two thicknesses l_1 and l_2, respectively, A_R is the ratio of the PA amplitudes, and $\Delta\phi = \phi_s(l_1) - \phi_s(l_2)$ the phase difference.

As one can see, this ratio is a function only of the sample thermal, optical, and transport parameters and it is independent of the detecting system characteristic (microphone, PA cell, lock-in, chopper, etc.). Using our theoretical outcome and this kind of normalization, it was possible to investigate both thermal and electronic transport properties of a Ge single crystal.

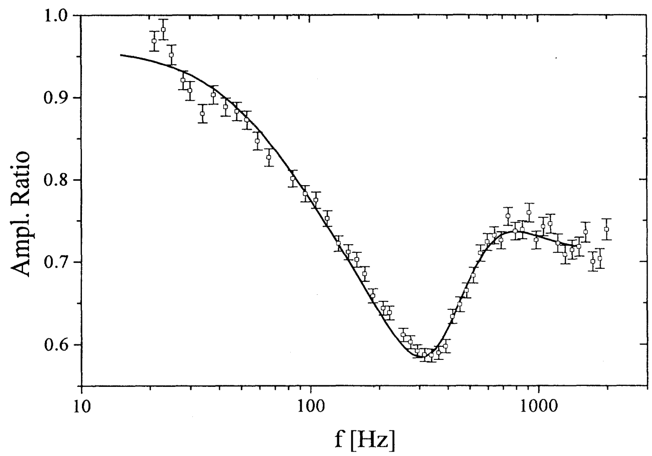

FIG. 5. PA amplitude ratio for two Ge sample thicknesses, $l_1 = 910\ \mu$m and $l_2 = 770\ \mu$m, as a function of the modulation frequency. In both measurements the polished side was in contact with the PA chamber. The solid line represents data fitting Eqs. (9) and (15).

In Figs. 4 and 5 we show the PA amplitude ratio (squares) for the Ge sample as a function of the modulation frequency for the case of a 1000 μm thick sample normalized with a 770 μm thick sample and a 910 μm thick sample normalized with a 770 μm thick sample. In both cases the sample surface in contact with air in the PA chamber, opposite to the illuminated surface, was highly, mirrorlike polished and the illuminated surface was roughened. In the frequency region where the thermalization component is dominant, up to ~ 200 Hz, the slope of the amplitude ratio is approximately given by $\exp\left[-(l_1 - l_2)\sqrt{\pi f/D_T}\right]$. This kind of slope can be pre-

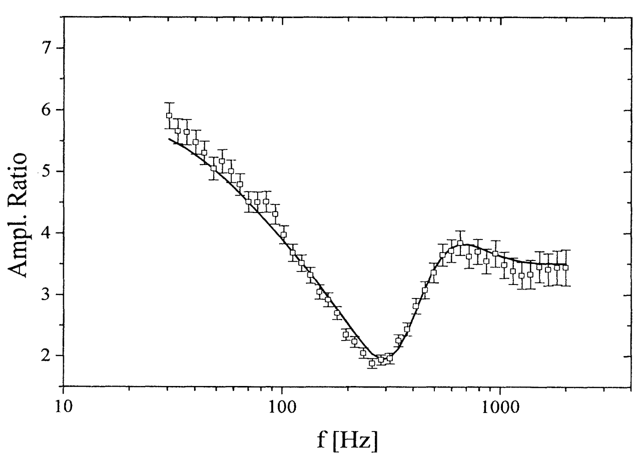

FIG. 4. PA amplitude ratio for two Ge sample thicknesses, $l_1 = 1000\ \mu$m and $l_2 = 770\ \mu$m, as a function of the modulation frequency. In both measurements the polished side was in contact with the PA chamber. The solid line represents data fitting Eqs. (9) and (15).

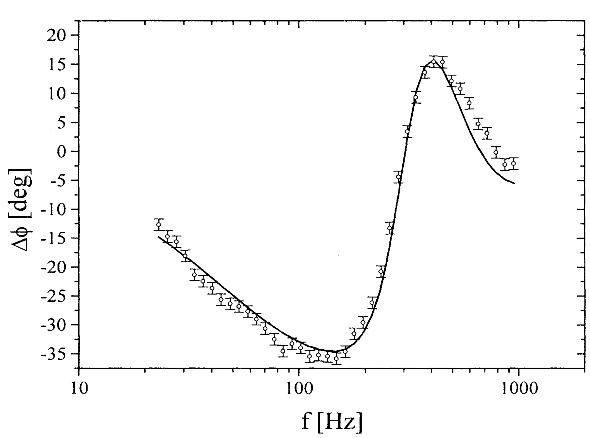

FIG. 6. PA phase angle difference $\Delta\phi$ for two Ge sample thicknesses, $l_1 = 1000\ \mu$m and $l_2 = 770\ \mu$m, as a function of the modulation frequency. In both measurements the polished side was in contact with the PA chamber. The solid line represents data fitting Eqs. (9) and (15).

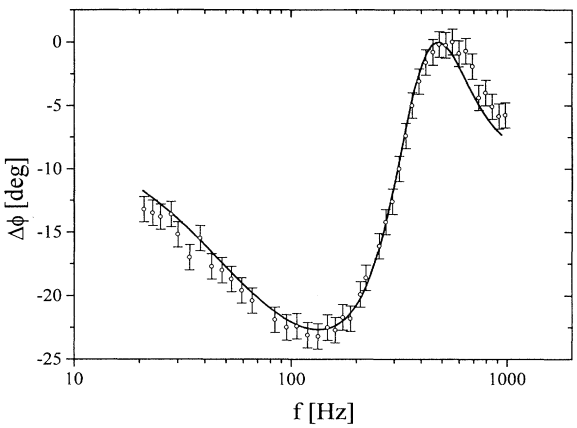

FIG. 7. PA phase angle difference $\Delta\phi$ for two Ge sample thicknesses, $l_1 = 1000$ μm and $l_2 = 770$ μm, as a function of the modulation frequency. In both measurements the polished side was in contact with the PA chamber. The solid line represents data fitting Eqs. (9) and (15).

dicted using the RG (Ref. 9) theory with an instantaneous heat source. For frequencies higher than ~ 800 Hz the amplitude ratio is in the saturation region. In this frequency region recombination components (nonradiative bulk and surface recombinations) are dominant and the amplitudes of all three components, for thicknesses of 1000 μm, 910 μm, and 770 μm, have the same slope and the ratio is constant.

In Figs. 6 and 7 we show the PA phase difference $\Delta\phi$ (circles) for the Ge sample as a function of the modulation frequency for the previous measurements. In the frequency region up to ~ 100 Hz $\Delta\phi$ corresponds to $-(l_1 - l_2)\sqrt{\pi f/D_T}$.

Using Eqs. (9) and (15) together with the value of D for Ge (D=44 cm^2/s was calculated from the value of the Hall mobility using the Einstein relation $D_{n(p)} = \mu_{n(p)} k_B T/e$), we have fitted the PA phase and amplitude data for both ratios, 1000 versus 770 μm and 910 versus 770 μm, in the complete frequency range. In Figs. 4 and 5 the solid line represents the best fit to the data of Eqs. (9) and (15), using the calculated value for D, leaving D_T, τ, and s_b as fitting parameters. Similarly, in Figs. 6 and 7 we present, with the solid line, the best fit to the phase angle of Eqs. (9) and (15). In Table I the values found for adjustable parameters, D_T, s_b, and τ are summarized for two ratios and both amplitude and phase, together with the minimum fitting steps. The error estimates were calculated using the method presented in Ref. 11 Chaps. 10 and 14, and they are also presented in Table I. The values obtained for the thermal diffusivity, as shown in Table I, are in very good agreement for all four fitting procedures with the literature value[12] of 0.37 cm^2/s for Ge. All four values obtained for the relaxation time are very close to each other and agree quite well with the literature value for that doping concentration (Ref. 13) which is ~ 20 μs. Finally, we note that the values obtained for the surface recombination velocity on the back side of the sample are expected for surfaces prepared as mentioned in Sec. III. One can see that for all obtained parameters the error estimates associated with these measurements bring the data into agreement for two sample thickness ratios.

To investigate the influence of each component we have plotted all three components, T, NRR and SR, together with their total. The values for τ, D_T, D, and s_b were used from Table I. In Fig. 8 the full line represents the total PA signal amplitude and the dotted, dashed, and dotted-dashed lines represent bulk recombination, surface recombination, and thermalization components of the PA signal amplitude. One can see that three general regimes exist: the first for frequencies up to 200 Hz where the thermal component is dominant and the amplitude has an exponential slope. The second regime is dominated by carrier transport behavior, in our particular case the surface recombination component of the back side [second term in Eq. (12c)]. These two regimes are most clearly seen at low and high modulation frequencies, respectively. The third domain is for intermediate frequencies, where there is a complex interaction that is highly sensitive to the excess carrier lifetime and surface recombination velocities.

V. CONCLUSION

In this paper we have carried out a modulation frequency investigation of the PA signal, in the heat-transmission configuration, of Ge single crystals. A one-dimensional model which predicts the PA amplitude and phase was developed allowing the determination of both thermal and electronic transport properties of intrinsic or near intrinsic semiconductors for heat-transmission and heat-reflection configuration, and with small modifica-

TABLE I. The Ge single crystal transport parameters.

Ratio (μm/μm)	Fitted (phase or amplitude)	Thermal diffusivity (cm^2/s)	Surface recombination velocity (cm/s)	Relaxation time (μs)
	Tolerance	0.005	10	0.1
910/770	Amplitude	0.395 ± 0.020	1070 ± 70	19.8 ± 1.5
910/770	Phase	0.390 ± 0.015	1020 ± 50	20.5 ± 1.0
1000/770	Amplitude	0.385 ± 0.020	960 ± 70	19.8 ± 1.5
1000/770	Phase	0.370 ± 0.015	940 ± 50	19.8 ± 1.0

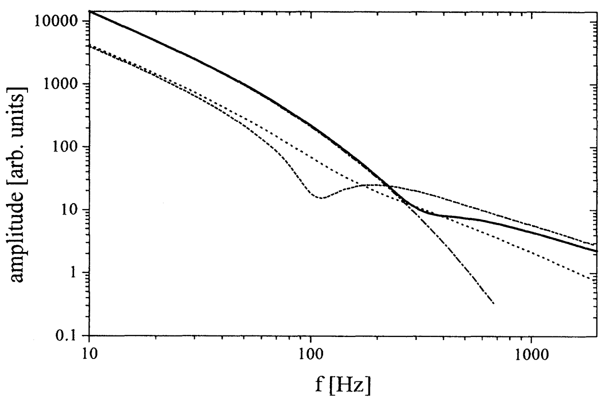

FIG. 8. Theoretical PA signal amplitude vs modulation frequency (solid line) and thermalization (dot-dashed line), and nonradiative bulk recombination (dotted line) and nonradiative surface recombination (dashed line) components calculated using average parameters from Table I for sample thickness $l = 1000$ μm.

tions for the photobeam deflection technique. The optical absorption coefficient was treated as finite, which caused the absorption through the sample volume rather than just the surface absorption process. Then, it is possible to use these relations for analyzing thin films deposited on a transparent substrate, because although $E_g > E$ and the absorption coefficient is high, due to the small film thickness the condition $\exp(-\sigma_s l)$ is not fulfilled. To eliminate the influence of the frequency characteristic of the measuring system we have normalized our signal with a sample measured at different thicknesses. From both the phase and amplitude signals, as a function of the modulation frequency, in the complete frequency region the room-temperature values of important semiconductor parameters such as surface recombination velocity and the nonradiative recombination time were obtained quantitatively.

Finally, with the simple heat-transmission configuration we have demonstrated the usefulness of both amplitude and phase data to obtain both transport and thermal parameters of semiconductors and we have suggested a method to eliminate the frequency characteristic of the measuring system which can lead to errors in the determination of the measured parameters.

ACKNOWLEDGMENTS

This work was supported by the SMST under Contract No. 1001E. The authors gratefully acknowledge Mr. A. Rakić for helpful discussions.

[1] L. F. Perondi and L. C. M. Miranda, J. Appl. Phys. **62**, 2955 (1987).

[2] M. O. Silva, I. N. Bandiera, and L. C. Miranda, J. Phys. E **20**, 1476 (1987).

[3] V. A. Sablikov and V. B. Sandomirskii, Phys. Status Solidi **120**, 471 (1983).

[4] S. O. Ferreira, C. Ying An, I. N. Bandeira, L. C. Miranda, and H. Vargas, Phys. Rev. B **39**, 7967 (1989).

[5] D. Fournier, C. Boccara, A. Skumanich, and N. M. Amer, J. Appl. Phys. **59**, 787 (1986).

[6] J. Pelzl, D. Fournier, and C. Boccara, in *Photoacoustic and Photothermal Phenomena*, edited by P. Hess and J. Pelzl, (Springer-Verlag, Berlin, 1988), p. 241.

[7] A. Pinto Neto, H. Vargas, N. F. Leite, and L. C. Miranda, Phys. Rev. B **40**, 3924 (1989).

[8] A. Pinto Neto, H. Vargas, N. F. Leite, and L. C. Miranda, Phys. Rev. B **41**, 9974 (1990).

[9] A. Rosencwaig and A. Gersho, J. Appl. Phys. **47**, 64 (1976).

[10] J. P. McKalvey, *Solid State and Semiconductor Physics* (Harpers & Row, New York, 1966).

[11] W. H. Press, B. P. Flannery, S. A. Tenkolsky, and W. T. Vetterling, *Numerical Recipes, The Art of Scientific Computing* (Cambridge University Press, Cambridge, 1986).

[12] *CRC Handbook of Chemistry and Physics*, 69th ed., edited by Robert C. Weast (CRC, Boca Raton, 1989).

[13] S. Wang, *Solid State Electronics* (McGraw-Hill, New York, 1985).

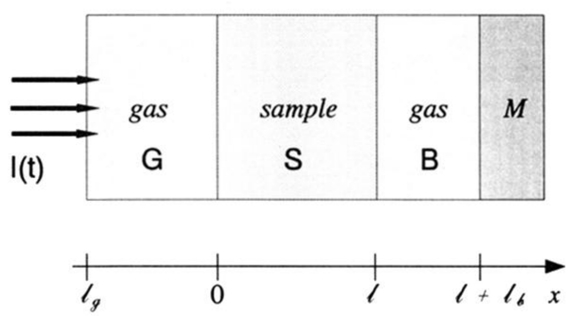

FIG. 1. PA cell geometry for the heat-transmission configuration.